Community composition and strain identity drive metabolic competition and *Staphylococcus aureus* colonization resistance in Synthetic Nasal Communities

Marcelo Navarro Diaz[1,2,3], Laura Camus[1,2], Soyoung Ham[2,4], Lars Angenent[2,4,5,6,7], Simon Heilbronner[1,2], Paolo Stincone[1,2], Johanna Rapp[1,2,3], Daniel Petras[1,2,8*], Hannes Link[1,2,3*]

[1] Interfaculty Institute of Microbiology and Infection Medicine, University of Tübingen, 72076 Tübingen, Germany

[2] Cluster of Excellence "Controlling Microbes to Fight Infections", University of Tübingen, 72076 Tübingen, Germany

[3] M3 Research Center, University of Tübingen, Otfried-Müller-Str. 37, 72076 Tübingen, Germany

[4] Environmental Biotechnology Group, Department of Geosciences, University of Tübingen, Schnarrenbergstraße 94-96, 72076 Tübingen, Germany

[5] Max Planck Institute for Biology Tübingen, Max-Planck-Ring 5, 72076 Tübingen, Germany

[6] Department of Biological and Chemical Engineering, Aarhus University, Gustav Wieds Vej 10D, 8000 Aarhus C, Denmark

[7] The Novo Nordisk Foundation CO2 Research Center (CORC), Aarhus University, Gustav Wieds Vej 10C, 8000 Aarhus C, Denmark

[8] Department of Biochemistry, University of California, Riverside, 169 Aberdeen Dr., Riverside, CA 92507, USA

* Corresponding authors: dpetras@ucr.edu, hannes.link@uni-tuebingen.de

Abstract

The human nasal microbiome is a low-diversity ecosystem whose assembly principles and mechanisms of colonization resistance remain poorly understood. In particular, *Staphylococcus aureus* colonization shows high heterogeneity across individuals. We hypothesized that nutritional competition, strain-level diversity, and nutrient availability shape community stability and the ability of commensal species to inhibit *S. aureus*. To test this, we constructed 50 defined synthetic communities composed of representative human nasal bacteria differing in strain and species composition and tracked their temporal dynamics, metabolic profiles, and nutritional interactions. The composition of synthetic communities with 5-10 species showed robust and reproducible dynamics and converged in one of three stable states. Synthetic communities dominated by a specific strain of *Corynebacterium propinquum* were highly stable and consistently excluded *S. aureus*. Growth and coculture assays showed that *C. propinquum* outcompetes *S. aureus* under poor nutritional conditions resembling the nasal environment, whereas *S. aureus* dominates in nutrient-rich conditions. Metabolomics analyses revealed that nutritional competition, including siderophores utilization and amino acid limitation, likely underlies this colonization resistance. These results establish a tractable synthetic community model for the human nasal microbiome and identify nutrient-dependent competition and microbial metabolite production as key drivers of community structure and pathogen exclusion.

53 **Introduction**

54 The human microbiome is important for human health and provides protection against
55 pathogens. This colonization resistance can occur through various mechanisms such
56 as nutritional competition or by use of inhibitory compounds [1]. Each anatomical site
57 contains distinct microbial communities composed of commensals, pathobionts, and
58 pathogens, which may be permanent residents or transient colonizers. Among these
59 sites, the nasal cavity is of particular interest because it is an entry point of airborne
60 pathogens such as *Staphylococcus aureus*, which is a major human pathobiont [2].
61 Approximately one-quarter of adults are persistently colonized with *S. aureus* in the
62 anterior nares, while others are intermittently colonized or remain uncolonized [3]. In
63 S. aureus carriers, the nasal cavity functions as a reservoir from which *S. aureus* can
64 disseminate to other body sites, occasionally leading to disease [4], which is especially
65 dangerous in immunocompromised and post-operation patients [5, 6].

66

67 Despite its clinical importance, the ecological and mechanistic factors that determine
68 the presence, absence, or abundance of *S. aureus* in the nasal microbiome are not
69 completely understood. Colonization resistance to *S. aureus* in the nose is a complex
70 process where the host's immunity has been show to play a role [7] and several species
71 present in the nasal microbiome have been to show different types of interactions with
72 *S. aureus*. Some examples of species that have been found to inhibit the growth of *S.*
73 *aureus* include *Staphylococus lugdunesis* (which produces the antimicrobial lugdunin),
74 *Staphylococcus epidermidis* [8] or *Dolosigranulum pigrum* [9]. Other important
75 mechanisms of *S. aureus* exclusion besides antimicrobials, includes nutrient depletion
76 [10, 11] and siderophore production [12]. Such nutritional competition is especially
77 relevant in the context of the poor availability of carbon sources and trace metals such
78 as iron in the nasal environment, which has been shown to be nutrient-limited and iron-

restricted, shaping microbial interactions and colonization dynamics [10, 13]. However, disentangling these mechanisms in vivo and in the context of a whole microbial community is challenging, as the nasal cavity is a highly heterogeneous and host-specific environment specific environment that supports a comparatively small but highly specialized microbial community [14, 15].

By using synthetic communities (SynComs), the low-diversity nasal microbiome provides an ideal model to study fundamental ecological processes such as community assembly, metabolic cross-feeding, and invasion dynamics under clinically relevant conditions. SynComs have been widely used for some time to model other microbiome systems, such as the human gut microbiome [16, 17] and the rhizosphere of plants [18, 19]. These model systems have been instrumental in dissecting mechanisms of community assembly [18, 20], microbial function metabolic interactions [21, 22], and the response of microbial consortia to perturbations such as antibiotics or pathogen invasion [19, 23]. To date, no SynCom has been reported for the human nasal microbiome. Previously, the PNC8 SynCom was developed to model the piglet nasal microbiome [24], but an analogous, experimentally tractable SynCom for the human nasal ecosystem is lacking. Here, we sought to establish synthetic nasal communities and investigate their resistance to invasion by *Staphylococcus aureus*.

Therefore, we developed a set of synthetic communities using a previously reported culture collection of human nasal isolates [25]. We assembled 50 SynComs containing random combinations of the most prevalent nasal bacterial species, each represented by three phenotypically distinct strains, and cultured them on agar plates with synthetic nasal medium which was previously development to resemble the nutritional conditions in the nose [10]. These cultures were propagated 3 times in fresh medium every three

105 days. During the last propagation, we added *S. aureus* to test their colonization
106 resistance. We characterized their compositional and metabolic profiles using long-
107 read amplicon sequencing and untargeted and targeted metabolomics. Our approach
108 allowed us to identify key species, strain-level effects, and metabolite signatures that
109 are associated with abundance of *S. aureus* in the SynComs. These results provide a
110 tractable in vitro system to explore the ecological determinants of nasal community
111 assembly and pathogen exclusion.
112
113 **Methods**
114 *Bacterial pool selection*
115 To select species for SynCom construction, we first analyzed the Human Microbiome
116 Project (HMP) 16S rRNA amplicon sequencing data from the nasal cavity body site
117 [26]. Raw sequences were processed using QIIME 2 v2021.11 [27]. Quality filtering,
118 denoising, and chimera removal were performed with DADA2 [28], followed by
119 inference of amplicon sequence variants (ASVs). Taxonomic assignment was carried
120 out using BLAST [29] against the NCBI 16S rRNA RefSeq database [30]. The complete
121 OTU table is provided in Supplementary Table S1.
122 Experiments were performed using bacterial isolates from the LaCa collection of nasal
123 bacterial isolates [25]. We selected 10 of the most prevalent species based on our
124 HMP analysis (Supplementary Figure 1), with the limitation that they were available in
125 the LaCa collection and selecting 3 strains per species isolated from different
126 volunteers to ensure that no two isolates belonged to the same population.
127
128 *SynCom cultivation*
129 Fifty synthetic communities (SynComs) were assembled by randomly selecting both
130 the number (from 5 to 10) and identity of species, along with one randomly chosen

strain per species. The experimental workflow is depicted in (Figure 1), and species/strains used in each SynCom are listed in Supplementary Table 2.

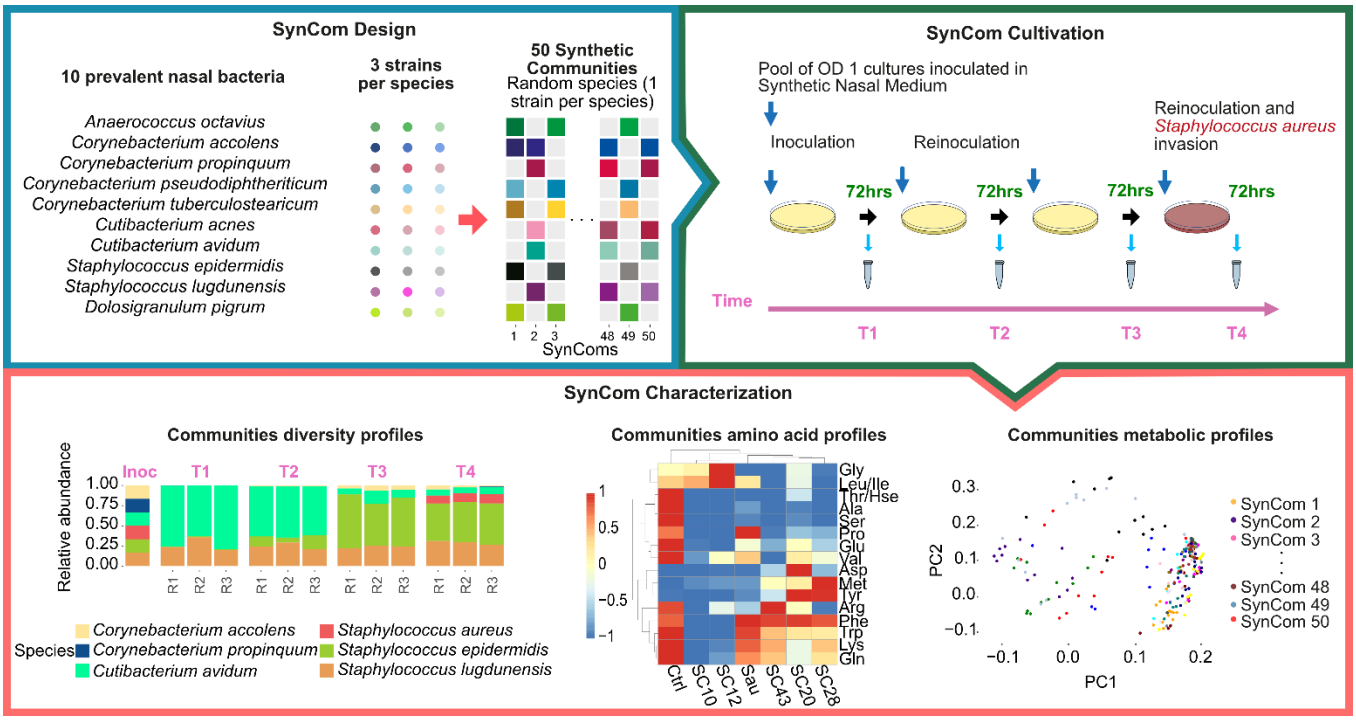

Figure 1. SynCom design and experimental workflow. Ten of the most prevalent nasal bacterial species, each represented by three strains, were selected based on analyses of Human Microbiome Project data and the strain availability in the LaCa collection of nasal isolates [25]. SynComs were designed by randomly selecting both the number and identity of species per community, followed by the random selection of one strain per species [25]. SynComs were cultivated on Synthetic Nasal Medium agar plates (SNM3; [10]). SynComs were inoculated and grown for 72 hours, after which, biomass samples were collected for reinoculation, DNA extraction and sequencing, and metabolomics. Three sequential reinoculations on fresh SNM3 plates were performed. In the final reinoculation, *S. aureus* was introduced to assess SynCom colonization resistance. SynCom composition was determined using Nanopore sequencing. Selected communities were further analyzed using targeted and untargeted metabolomics.

148

149 Starter cultures were grown from glycerol stocks 24–72 h before experiments using
150 BHI, LB, or Columbia agar plates, depending on species (Supplementary Table 3).
151 Bacterial biomass was harvested with sterile swabs, resuspended in PBS, and
152 adjusted to OD_{600} 1. Equal volumes (100 µL) of each strain suspension were pooled
153 to generate the SynCom inoculum.

154

155 SynComs were plated in triplicate on Synthetic Nasal Medium 3 (SNM3) agar plates,
156 designed to mimic human nasal secretions [10], and incubated for 72 h at 34 °C.
157 Inoculation of pooled cultures was made in 3 SNM3 plates to obtain 3 technical
158 replicates per SynCom. Biomass was collected with sterile loops using a star pattern
159 across the plate. Then, biomass was resuspended in 500 µL PBS and used for
160 reinoculation and DNA extraction. The rest of the biomass in the plate was collected
161 for metabolomics by transferring it into tubes containing 1 mL of 80% methanol and
162 storing them at −80 °C until processing. Reinoculation consisted of diluting the PBS
163 suspension to OD_{600} 1 and plating 100 µL on fresh SNM3 plates. This process was
164 repeated for three sequential transfers. In the final transfer, SynComs were challenged
165 with *S. aureus* by mixing 90 µL of the SynCom inoculum with 10 µL of an *S. aureus*
166 USA300 culture at OD_{600} 0.1 before plating (final inoculation OD_{600} for *S. aureus*
167 USA300 was 0.01).

168

169 *Repetition experiment*

170 To evaluate reproducibility and analyze metabolites consumption profiles, five
171 SynComs were cultivated in a separate experiment using 12-well plates containing 2
172 mL of SNM3 agar per well. Culture initiation and sampling followed the same procedure
173 as in the main experiment, except that 20 µL of inoculum was used per well. Biomass

174 was collected from the wells for DNA extraction and reinoculation. For targeted
175 metabolomics, biomass was extracted by flooding from the wells with 2mL of 80%
176 methanol, incubated at −20 °C for 20 min, and processed as described above. Three
177 biological replicates were used for each SynCom. Additionally, *S. aureus* USA300 and
178 the three strains of *C. propinquum* were also grown in 12-well plates to analyze their
179 metabolome.
180
181 *Cocultures*
182 To test how the nutritional environment affected the interaction between *C. propinquum*
183 and *S. aureus*, we performed cocultures between the 3 strains of *C. propinquum* used
184 in the SynCom experiments and *S. aureus* USA300. For these cocultures we used
185 SNM3, SNM10 (which contains 10x the amino acid concentration of base SNM) and
186 the rich-nutrient medium BHI. We followed the same inoculation protocol of the
187 SynCom experiment and incubated 72 hours at 34°C after which we took biomass
188 samples for DNA extraction and sequencing. Three biological replicates were used for
189 each of the cocultures.
190
191 *Growth curves*
192 To analyze the differences in the grow of *C. propinquum* under different nutritional
193 conditions we performed growth curves for each of the 3 strains of *C. propinquum*
194 strains used in the SynCom experiments in SNM3, SNM10 and BHI. Biomass from
195 reactivated strains was transferred using an inoculation loop to BHI medium in a 5 ml
196 culture tube and incubated for 48h with shaking at 220 rpm and at 37°C. After 48h, the
197 turbidity was assessed to ensure sufficient growth before transferring 1.8 ml of medium
198 to a sterile 2 ml Eppendorf tube. For growth curves in SNM3 and SNM10, the cells
199 were then washed twice in SNM salts base (SNM without glucose or amino acids). The

200 OD was adjusted to 0.02 and cultures were transferred to a flat bottom 96-well plates.
201 Cultures were incubated at 37°C and shaken continuously at 269 cpm (6 mm). The OD
202 was measured every 10 minutes for 72 hours.
203
204 *Sequencing analyses*
205 DNA was extracted using the ZymoBIOMICS DNA Miniprep Kit (Zymo Research Corp.,
206 Irvine, CA, USA) following the manufacturer's protocol. Full-length rRNA operon
207 amplicons (~4,000 bp) were generated by PCR using primers 16S-27F-GGTGCTG-
208 ONT and 23S-2241R-GGTGCTG-ONT as described previously [31]. Nanopore
209 sequencing libraries were prepared with the Rapid Barcoding Kit (SQK-RBK114.96)
210 following the "Amplicon sequencing from DNA protocol" (available at
211 https://nanoporetech.com/document/rapid-sequencing-v14-amplicon-sequencing-
212 sqk-rbk114-24-or-sqk) and sequenced on MinION V14 flow cells (Oxford Nanopore
213 Technologies) using MinKNOW v25.05.14. Only reads with a quality score ≥10 were
214 retained and demultiplexed. Taxonomic classification was performed using Emu v3.4.5
215 [32] with a custom rRNA operon reference database generated from the strain
216 genomes via in silico PCR using EMBOSS-primersearch [33] as previously reported
217 [31].
218
219 Initial screening involved sequencing one replicate of the final time point (i.e. after *S.*
220 *aureus* invasion) for each of the 50 SynComs. The complete OTU table is provided in
221 Supplementary Table S4. Twenty representative SynComs were then selected for
222 sequencing of all time points and replicates. The complete OTU table is provided in
223 Supplementary Table S5. Out tables for the repetition experiment and coculture
224 experiments are available as Supplementary Table S6 and Supplementary Table S7

225 respectively. Raw fastq files from sequencing data are available in the NCBI SRA
226 database under the BioProject PRJNA1370791.
227
228 *Untargeted metabolomics*
229 For 20 selected SynComs, scrapped biomass from agar plates extracted in 80%
230 methanol was sonicated for five cycles (60s on, 10 s off, 40% amplitude), centrifuged
231 (10,000 rpm, 10 min), and supernatants were transferred to pre-weighed glass vials.
232 Methanol was evaporated under vacuum, and dried extracts were weighed and
233 resuspended to 5 mg/μL in 80% methanol.
234
235 Chromatographic separation was performed on a UHPLC system equipped with a C18
236 core-shell column (50 × 2.1 mm, 1.7 μm; Phenomenex). Solvent A was H_2O + 0.1%
237 formic acid, and solvent B was acetonitrile + 0.1% formic acid. The gradient increased
238 from 5% to 50% B over 8 min, then to 99% B by minute 10, followed by washing and
239 re-equilibration. Mass spectrometry was conducted on a Q-Exactive HF using heated
240 electrospray ionization in positive mode. MS1 scans were acquired at 60,000
241 resolution (120–1500 m/z). Data-dependent MS2 (Top 5) was performed with stepped
242 normalized collision energies of 25/35/45. Data were centroid-transformed and
243 processed with MZmine4 v4.2.0 [34], and molecular networking was performed in
244 GNPS 2 [35]. Chemical classification was inferred using CANOPUS [36] and SIRIUS
245 [37]. The full feature table is available in Supplementary Table S8 and SIRIUS
246 annotations are available in Supplementary Table S9. Raw data for untargeted
247 metabolomics is available in MassIVE with accession number MSV000096776.
248
249
250

251 *Targeted metabolomics of metabolites*

252 Methanol extracts from the 12-well plates experiment were recovered, centrifuged, and
253 stored at −80 °C until analysis. Metabolites were quantified by isotope-ratio LC-MS/MS
254 on an Agilent TQ 6495 using a HILIC-Z column (2.1 × 150 mm, 2.7 µm; Agilent).
255 Chromatographic parameters followed Agilent application note 5994-5949. The full
256 feature table is available in Supplementary Table S10.

257

258 *Statistical analyses*

259 Amplicon data were analyzed in *R* v4.4.0 (using RStudio v2024.12.1). SynComs were
260 clustered based on relative abundances at the final time point using partitioning around
261 medoids (PAM) clustering implemented in the *cluster* R package [38]. The optimal
262 number of clusters was automatically determined using the Silhouette method [39],
263 selecting the number of clusters that maximized average silhouette width. Differential
264 metabolite abundance between SynCom clusters was analyzed using the *limma*
265 package [40]. Intensities were $\log_2$-transformed and quantile-normalized. Linear
266 models were fitted for each metabolite, and empirical Bayes moderation was applied
267 to obtain moderated t-statistics, $\log_2$ fold-changes, and Benjamini–Hochberg FDR-
268 adjusted p-values. Metabolites with FDR < 0.05 and $|\log_2 FC| > 1$ were considered
269 significantly associated with SynCom clusters. Multi-omics data integration and
270 visualization were performed in R using ggplot2 [41].

271

272 **Results**

273 *Nasal SynComs reflect the compositional diversity of the human nasal microbiome*

274 To develop synthetic communities that resemble the nasal microbiota, we used 10
275 bacterial species, each represented by 3 different strains, each isolated from healthy

individuals (Figure 1). We selected these 10 bacterial species because they include some of the most prevalent bacteria in the human nasal microbiome (Figure S1).

Next, we assembled 50 SynComs by randomly selecting 5 to 10 species and one random strain per species. These were grown individually, then adjusted to an optical density of 1 and mixed in equal ratios. These seed cultures were then used to inoculate agar plates with synthetic nasal medium (Figure 1). The SynComs were grown for 3 days and transferred to fresh plates to ensure sufficient supply with nutrients. To evaluate the stability and assembly process of the SynComs, the reinoculation was performed 3 times and on the last reinoculation *S. aureus* was added to test for the colonization resistance of the SynComs. Next, we used Nanopore long-read amplicon sequencing (16S RNA) to characterize the composition of the communities at the final time point (i.e. after *S. aureus* was added, Figure 1). The composition of the 50 SynComs clustered in three distinct groups (Figure 2, compositional similarity with silhouette method). These three clusters showed different compositional characteristics (i.e., species richness, evenness, and dominant species; Figure 2). Moreover, they showed different resistance to *S. aureus* colonization at the end of the experiment (Figure 2).

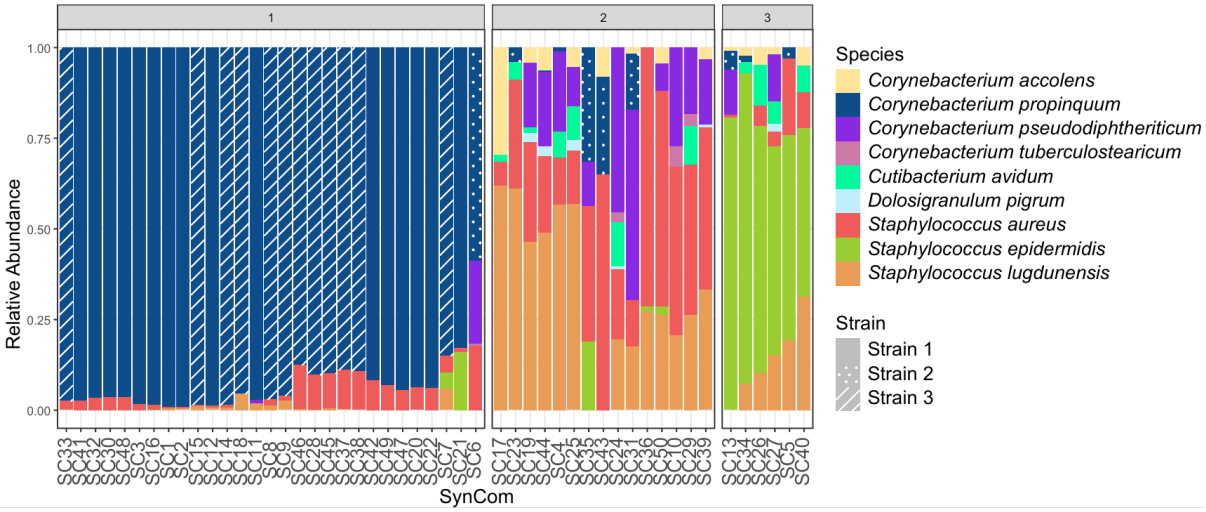

Figure 2. Screening of SynComs based on microbial composition at the final time point. For each of the 50 SynComs assembled, one replicate was characterized at the final time point (72 hours after *S. aureus* inoculation). SynComs were clustered based on similarity in microbial composition. Relative abundance was calculated per sample and used to compute Euclidean distances, followed by clustering. The optimal number of clusters (3) was determined automatically using the silhouette method. Each panel shows the relative abundance of all species detected in the 50 SynComs. For *C. propinquum* and *D. pigrum* the different strains are indicated by barplot patterns. Strain level information of other species is not shown.

Cluster 1 was dominated by *C. propinquum* (mean of 93.1%) and showed high resistance to *S. aureus* (mean abundance of 4.6%, Figure 2). Just a few other species occurred at low abundance in cluster 1 SynComs (e.g. *Staphylococcus lugdunensis* and *S. epidermidis*). Thus, the 20 SynComs of cluster 1 consisted primarily in co-cultures of *C. propinquum* and *S. aureus*. The other two clusters showed higher species diversity. Cluster 2 frequently included *S. lugdunensis*, *C. pseudodiphtheriticum*, *C. avidum*, *D. pigrum*, *C. accolens*, and *C. tuberculostearicum*. This cluster had the lowest colonization resistance, with a mean relative abundance of

314 *S. aureus* of 34.1%. Cluster 3 included similar species as cluster 2 but was dominated
315 by *S. epidermidis* and *S. lugdunensis*. Cluster 3 showed strong colonization resistance,
316 with a mean final relative abundance of *S. aureus* of 6.9%. Two bacterial species *A.*
317 *octavius* and *C. acnes* were not detected in any SynCom.
318
319 *Strain-level diversity influenced population dynamics and resistance to S. aureus*
320 *colonization*
321 Next, we selected 20 representative SynComs that captured the compositional
322 diversity of the full data set. We characterized their composition at all time points, which
323 included the 4 samples taken every 72 hours when sampling for biomass to
324 reinoculated the SynComs in fresh SNM3 plates. For these SynComs, we sequenced
325 all time points and replicates. Figure 3 shows one replicate per SynCom and time point
326 and Supplementary Figure 2 A shows the Bray-Curtis distance between the replicates
327 which was below 0.2 for most of the SynComs indicating high replicability of the
328 experimental setup.
329

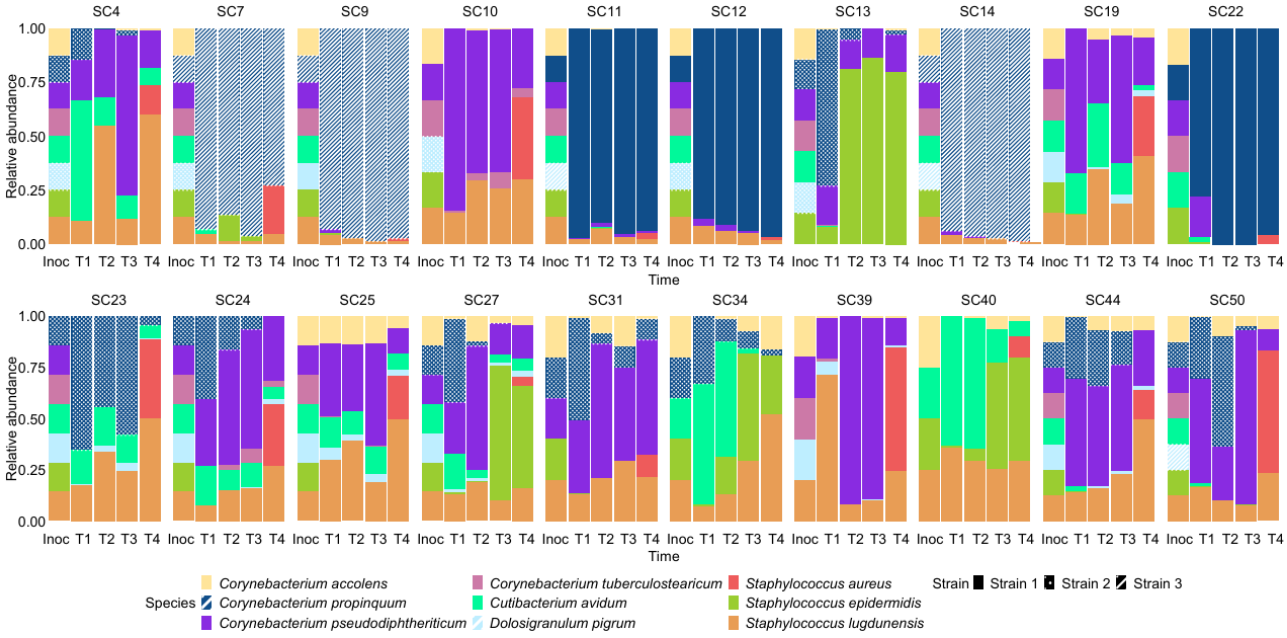

330

331 **Figure 3. Temporal dynamics of bacterial community composition in 20 selected**
332 **SynComs.** For 20 SynComs, community composition was characterized by
333 sequencing at four time points across the experiment. Each panel represents one
334 SynCom and shows relative abundance barplots for one replicate per SynCom over
335 time. Barplot patterns indicate which of the three strains was inoculated for *C.*
336 *propinquum* and *D. pigrum*.
337
338 Overall, our results revealed that both species and strain identity had a substantial
339 impact on SynCom composition. In addition to Figure 3, Supplementary Figure 2 B
340 shows the Bray-Curtis distance between the first three timepoints and the final
341 composition for all sequenced SynComs. In general, there were two types of assembly
342 patterns, one that stabilized quickly after timepoint 1 and another that varied at the 4
343 time points. The first group with fast stabilization, included SynComs that were
344 dominated by *C. pripinquum* strains 16 and 265. These SynComs showed low
345 dissimilarity values from the beginning of the experiment compared to the final state.
346 The other SynComs showed less stable dynamics with a more fluctuating composition
347 and higher dissimilarity values in respect to the final state, which was dependent on
348 the species and strains inoculated.
349
350 Next, we observed that strain-level variation played an important role for assembly of
351 the different SynCom. For example, the presence of distinct strains of the same
352 species had a strong effect on the abundance of *S. aureus* at the final time point. The
353 strongest strain-level effect was *C. propinqum* in cluster 1, in which all except for one
354 of the SynComs consisted of two *C. propinquum* strains (Nr. 16 and Nr. 265; Figure 2).
355 In contrast, *C. propiqnuum* strain 70 was present only during the first time points and
356 other species overgrew it by the end of the experiment (for example SynComs 13, 23

357 and 50, Figure 3). Thus, *C. propinquum* strain 70 only dominated in SynCom 6 (Figure
358 2). Similarly, *D. pigrum* strain 21 was the only strain of this species that could persist
359 through the entire cultivation period in the SynComs where it was included, although
360 its abundance was always below 5%. Notably, *D. pigrum* is a fastidious bacterium and
361 neither of the strains showed growth when we tried growing them as monocultures in
362 SNM3 (Supplementary Figure 4). Thus *D. pigrum* was only able to grow as part as
363 these specific SynComs. The other strains of *D. pigrum* were never detected after the
364 first reinoculation. Additionally, we observed co-occurrence patterns at species level
365 such between *C. accolens*, *C. avidum*, *C. pseudodiphtheriticum*, and *D. pigrum*,
366 independently of the strains used for the first two species (for example in SynComs 19,
367 25, 27, 44 and 50).
368
369 To explore how the nutritional environment affected the interaction between *C.*
370 *propinquum* strains and *S. aureus* USA300 we performed cocultures between the 3
371 strains of this species and *S. aureus*. *C. propinquum* strains 16 and 265, were able to
372 dominate over *S. aureus* under the nutritional conditions of SNM3 (Figure S3A). In BHI
373 medium, in contrast, *S. aureus* dominated the pair-wise co-cultures with all three *C.*
374 *propinquum* strains. Additionally, the *C. propinquum* strains 16 and 265 achieved
375 higher optical densities after 72 hours growth in liquid medium than strain 70 (Figure
376 S3B).
377
378 *Metabolome of SynComs differs between clusters and suggests nutritional competition*
379 To investigate metabolism of the different SynComs we performed untargeted
380 metabolomics on all time points and replicates of the 20 selected SynComs (Figure 4).
381 Metabolite extracts in methanol:water were collected from plates and analyzed by
382 untargeted LC–MS/MS enabling comprehensive detection of small-molecule features

383 without prior assumptions about metabolite identities. The resulting MS1 and MS2 data
384 were processed with MZmine4 and organized into feature-based molecular networks
385 through GNPS and classified with CANOPUS to aid in feature annotation and
386 interpretation.
387
388 We used Linear Models for Microarray Data (limma) to test whether the identified
389 SynCom clusters according to microbial composition (Figure 2 and Figure 4A) differed
390 in their metabolic profiles. Limma applies linear modeling and an empirical Bayes
391 method to detect features that differ significantly between predefined groups while
392 accounting for variance and multiple testing. This analysis showed that each cluster
393 has distinct metabolic signature (Figure 4B). Especially SynComs from cluster 1, which
394 were dominated by *C. propinquum*, showed enrichment of specific metabolites such
395 as the siderophore Deferroxamine E, thus indicating that this metabolite plays a role
396 for the high abundance of *C. propinquum* in these SynComs. Annotation with SIRIUS
397 predicted that the remaining compounds are mainly amino acids and derivatives and
398 peptides.
399

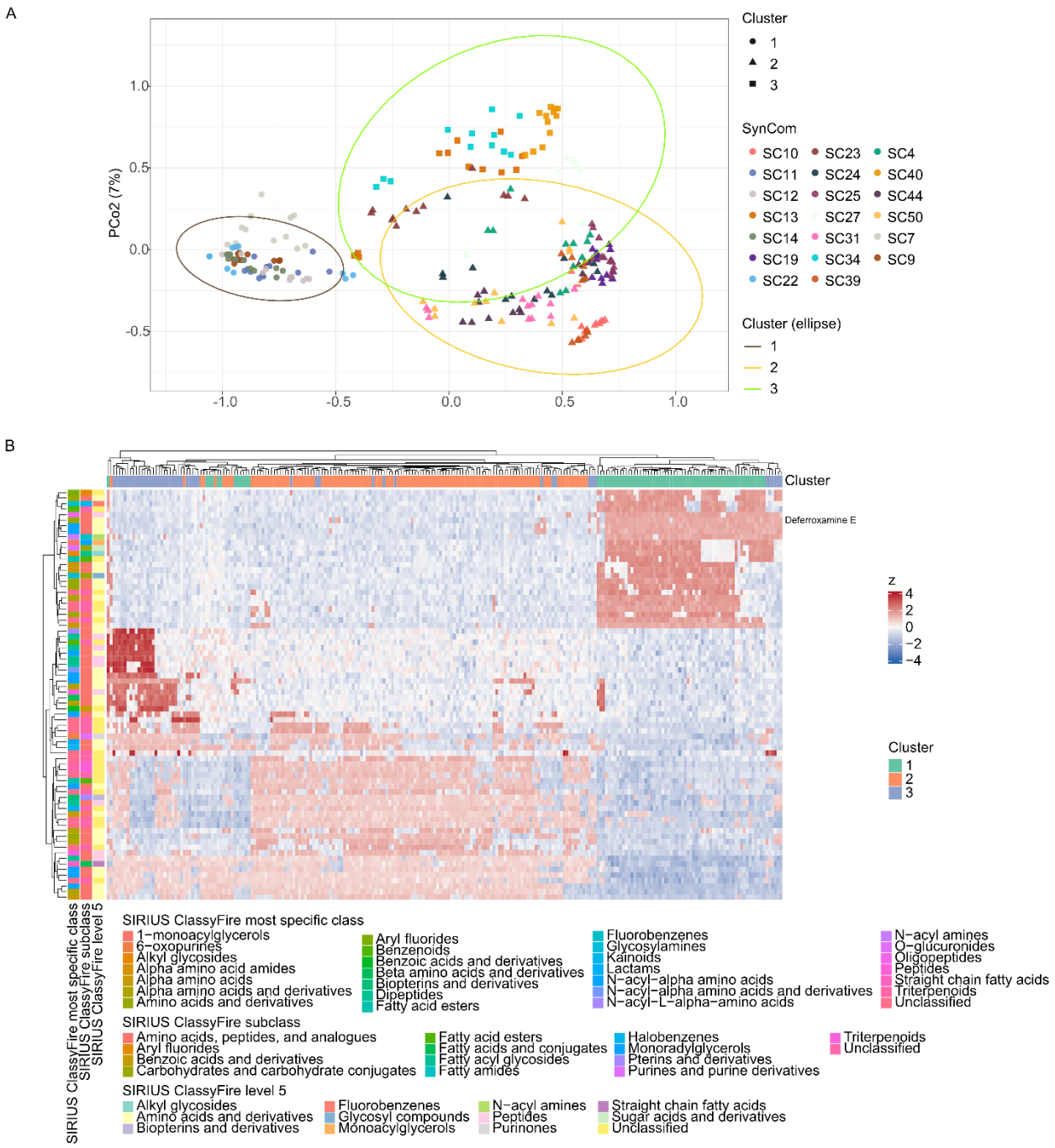

Figure 4. Compositional similarity and metabolic profiles of the 20 selected SynComs. (A) Principal coordinates analysis (PCoA) of bacterial community composition for samples from the 20 selected SynComs. The ordination is based on pairwise dissimilarities in relative abundances. Each point represents one sample; colors indicate SynCom identity, while point shapes and 95% confidence ellipses denote the SynCom composition clusters. (B) Heatmap of the top 30 metabolite

407 features associated with SynCom clusters, identified using a limma-based linear
408 modeling approach using the limma package for R [40]. The column annotation above
409 the heatmap indicates the cluster assignment of each sample. Row annotations on the
410 left indicate predicted metabolite classes as assigned by the SIRIUS CANOPUS
411 algorithm. Metabolite signals are displayed as standardized values (row-wise z-scores
412 of log-transformed intensities).
413
414 *Metabolites production and consumption profiles are SynCom-specific and influence*
415 *S. aureus colonization resistance*
416 To assess the role of amino acids and other metabolites on the nutritional competition
417 in community assembly and *S. aureus* colonization resistance, we analyzed a panel of
418 24 nutrients including amino acids, nucleosides and vitamins for 5 selected SynComs
419 (Figure 5 and Supplementary Table S10). Notably, when we cultured these 5 SynComs
420 for this metabolomics experiment their composition matched the results from the main
421 experiment, demonstrating the reproducibility of the cultivation protocol and SynCom
422 stability (Figure 5A). Additionally, we measured these compounds in *S. aureus*
423 USA300 that was used to test colonization resistance in the SynCom experiments and
424 in the three *C. propinquum* strains used in the SynCom experiments. Using 12-well
425 agar plates, we quantified concentration changes of the 24 nutrients relative to their
426 starting concentrations in the medium (Figure 5B and 5C). These data showed that
427 some nutrients are increasing relative to the medium, indicating that they are produced
428 by specific bacteria. For example, all 5 SynComs and the three *C. propinquum* strains
429 had high levels of riboflavin and tyrosine, which were hardly measurable in the medium
430 and in *S. aureus* cultures.
431

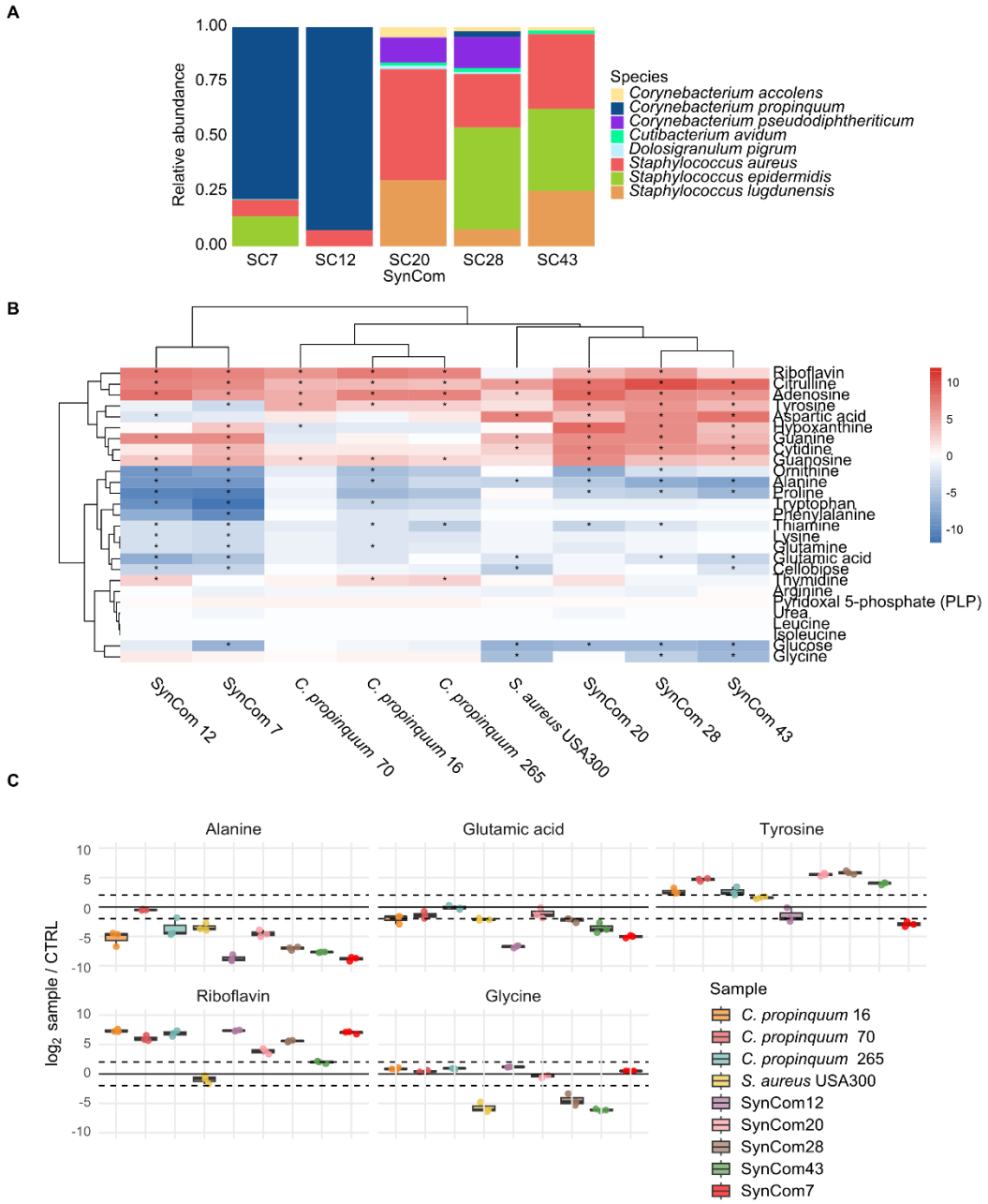

Figure 5. Bacterial composition and targeted metabolite profiles of five selected SynComs. Five SynComs selected from the main screen were regrown in 12-well plates to quantify metabolite production and consumption by targeted metabolomics. In parallel, monocultures of S. aureus USA300 (used to test colonization resistance) and the three *C. propinquum* strains were cultivated in the same format and analyzed alongside the SynComs. (A) Relative abundance barplots showing the bacterial composition of the five selected SynComs. (B) Heatmap of $\log_2$ fold-change in mean metabolite abundance relative to the medium-only control (SNM3 without inoculation).

441 For each metabolite and condition, $\log_2$ fold-changes were computed from mean
442 intensities across replicates. Asterisks indicate metabolites that differ significantly from
443 the control based on Welch's t-tests on $\log_2$-transformed replicate intensities with
444 Benjamini–Hochberg correction (FDR < 0.05) and an absolute $\log_2$ fold-change ≥ 2 (≥
445 4-fold change). (C) Boxplots showing $\log_2$ fold-change relative to the control for
446 selected metabolites that are strongly depleted by *S. aureus*. Each point represents an
447 individual replicate. The horizontal solid line at 0 indicates no change relative to the
448 control, while dashed lines at ±2 mark the 4-fold change thresholds. Colors denote
449 sample identity (SynComs and the individual bacterial monocultures).
450
451 Other nutrients were depleted in *S. aureus* cultures relative to the medium, such as
452 alanine, glutamic acid, and glycine. SynComs 10 and 12, which were dominated by *C.*
453 *propinquum*, showed strong decreases of several nutrients (at least 4-fold change in
454 10 out of 24 metabolites measured) including ornithine, Alanine, Proline, Tryptophane,
455 Phenylalanine, thiamine, Lysine, glutamine, glutamic acid (Figure 5B and 5C).
456 Similarly, SynComs 20, 28, and 43 showed high consumption of amino acids like
457 glycine, alanine, and glutamic acid.
458
459 **Discussion**
460 In this study, we used synthetic communities (SynComs) assembled from 10 prevalent
461 human nasal bacterial species (*Anaerococcus octavius*, *Corynebacterium accolens*,
462 *Corynebacterium propinquum*, *Corynebacterium pseudodiphtheriticum*,
463 *Corynebacterium tuberculostearicum*, *Cutibacterium acnes*, *Cutibacterium avidum*,
464 *Dolosigranulum pigrum*, *Staphylococcus epidermidis*, *Staphylococcus lugdunensis*).
465 This enabled us to investigate how community composition and strain-level variation
466 influence stability of these SynComs over time (four time points across 12 days) and

467 resistance to invasion of *S. aureus* at time point 4. Three distinct community clusters
468 emerged despite random species assembly, suggesting that deterministic ecological
469 processes play an important role in community assembly. These clusters can be
470 interpreted as three alternative stable states, each representing similar community
471 compositions, which different combinations of species and strains tend to converge
472 toward. Similar multistability has been documented across microbial communities,
473 where interaction-driven population dynamics and feedback loops generate alternative
474 taxonomic states [42, 43]. The clusters differed in species richness, evenness, and
475 dominant taxa, and showed markedly different levels of resistance to *S. aureus*
476 colonization. Notably, our panel of cultivated SynComs reproduced several
477 characteristics observed in the HMP dataset (Figure S1), particularly the frequent
478 coexistence of Corynebacterium species, the persistence of *D. pigrum*, and the overall
479 unevenness typical of nasal communities. Together, these findings demonstrate that
480 the ability of the nasal microbiome to resist *S. aureus* colonization can be recapitulated
481 and studied under controlled in vitro conditions, making our SynComs a platform for
482 systematic and mechanistic analyses of the nasal microbiota.
483
484 The observation that SynComs dominated by *C. propinquum* showed stronger
485 colonization resistance against *S. aureus* is consistent with previous studies showing
486 that nasal communities dominated by Corynebacterium spp. (including *C. propinquum*)
487 are often associated with reduced *S. aureus* carriage, potentially through production of
488 siderophores and other competitive factors that limit *S. aureus* growth [8, 11, 13, 44].
489 Analyses of HMP data supports this hypothesis and shows that species identities are
490 not the only predictive factor of colonization resistance. Our SynCom experiments
491 highlight two clear examples of strain-level effects: *C. propinquum* strains 16 and 265
492 consistently dominated SynComs, whereas strain 70 did not, and *D. pigrum* strain 21

493 was the only strain that could persist throughout the entire experiment. Together with
494 the high variability of *C. propinquum* abundance across the HMP cohort, ranging from
495 very low relative abundance to >70% in some individuals, these findings underscore
496 that strain-level characteristics are critical for nasal microbiome composition and
497 function. Interestingly, Corynebacterium species are prototroph for most amino acids,
498 cofactors, and vitamins and this biosynthetic capacity is conserved across species [45].
499 However, our data suggests that differences between strains still profoundly influences
500 their ability to dominate and persist, and future studies can clarify if this maps to
501 biosynthetic capacities of the different strains. For example, it has been shown that
502 mutations in biosynthetic genes can lead to strain-specific auxotrophies [46]. The same
503 is true for other species with reported inhibitory strains, such as *S. lugdunensis* [47] or
504 *D. pigrum* [9, 48].
505
506 *D. pigrum* is another key species in the nasal environment, ranking as the eighth most
507 prevalent species in the HMP cohort data. It has been noted as promoting colonization
508 resistance through modulation of the local microenvironment and production of
509 antimicrobial factors [9, 48]. Moreover, *D. pigrum* has been reported to engage in
510 positive interactions with Corynebacterium species, particularly *C.*
511 *pseudodiphtheriticum* [9, 49]. Our SynCom data support these observations, as *D.*
512 *pigrum* was only present in SynComs when *C. pseudodiphtheriticum* and *C. accolens*
513 were also present (SynComs 19, 25, 27, 44 and 50; Figure 2). While the mechanistic
514 basis of these associations remains unclear, understanding such cooperative
515 interactions is important given their potential synergistic effects against pathogens
516 such as *S. aureus*.
517

518 In addition to Corynebacteria and *D. pigrum*, staphylococcal species such as *S.*
519 *epidermidis* and *S. lugdunensis* are known to inhibit *S. aureus* through production of
520 antimicrobial peptides and direct interference [47, 50–52]. In our SynComs, rather than
521 observing isolated effects of individual species, we found evidence suggestive of
522 synergistic interactions between these two staphylococci due to their consistent
523 coexistence in the SynComs (SynComs 5, 7, 21, 26, 27, 34, 36, 40, 50; Figure 2). Such
524 cooperative effects have been described in previous research in the context of the
525 nasal environment and the respiratory tract, for example, synergism between *D.*
526 *pigrum* and *C. pseudodiphtheriticum* [49], or siderophore sharing between
527 staphylococcal species [44]. These results suggest that colonization resistance in the
528 nasal cavity is likely an emergent property of multiple interacting species and strains,
529 and this is likely influenced by both competition and cooperation.
530
531 Our metabolomics analyses provide additional insights into potential mechanisms
532 underlying colonization resistance. SynComs of cluster 1, dominated by *C.*
533 *propinquum,* were enriched in siderophore Deferrioxamine E which may deplete iron
534 and thus limit *S. aureus* growth. Previous studies have shown that iron sequestration
535 by siderophores is an important competitive mechanism of Corynebacteria in nasal
536 ecosystems [13, 44, 53, 54]. Moreover, we observed changes in the abundance of
537 nutrients like amino acids and riboflavin that were specific for some SynComs,
538 suggesting that nutrient competition may further contribute to colonization resistance.
539 We identified alanine, glutamic acid, tyrosine, glycine and riboflavin as important
540 nutritional metabolites for *S. aureus* USA300. These results are consistent with studies
541 reporting that *S. aureus* growth is constrained by amino acid availability in nutrient-
542 limited environments and by the fact that the nasal cavity is naturally poor in amino
543 acids [10, 25, 53].

544

545 Our pairwise coculture experiments with *C. propinquum* and *S. aureus* further support
546 the hypothesis that nutritional conditions influence the competitive dynamics between
547 the two bacteria. Under the poor nutritional conditions of SNM3, *C. propinquum* strains
548 16 and 265 successfully outcompeted *S. aureus*. In contrast, the nutrient-rich medium
549 BHI allowed *S. aureus* to overgrow all *C. propinquum* strains. These contrasting
550 outcomes suggest that differences in nutrient availability shape the relative fitness of
551 the two species.

552

553 One possible explanation is that *C. propinquum* is adapted to the nutritionally limited
554 environment of the nasal cavity, potentially favoring efficient resource utilization, while
555 *S. aureus* may be better suited to rapid growth under nutrient-rich conditions. Although
556 this hypothesis remains to be directly tested, it is consistent with expectations from r/K
557 selection theory [55] where the slow-growing K-strategists (in this case *C. propinquum*
558 *strains*) specialize in surviving under poor-nutrient conditions and r-strategists (*S.*
559 *aureus* in this scenario) maximize their growth rate in nutrient rich scenarios. r/K
560 strategies have been observed in other microbial systems, like soil communities, as
561 important for community structure and functioning [56, 57]. Further, this context-
562 dependent competitive outcome is a widely reported phenomenon, demonstrating that
563 competition for specific limiting nutrients, such as essential metal cofactors or amino
564 acids, mediates colonization resistance in diverse microbial systems like in the gut
565 microbiome against *Salmonella* [58]. Additionally, our observation that strains 16 and
566 265 grow better than strain 70 both in single and in SynCom cultures suggests that
567 intrinsic strain-level physiological differences are important factors of competitive
568 success. Together, these results indicate that both environmental constraints (e.g.
569 nutrient availability) and strain specific factors (e.g. biosynthetic capacities) determine

570 the ability of *C. propinquum* to inhibit *S. aureus*, providing a explanation for the strain-
571 dependent protection observed in our SynCom experiments.
572
573 The reproducibility of our SynCom approach shows that they are a tractable model
574 system for controlled and systematic investigations of nasal microbiome ecology. Until
575 now, most studies examining the effects of specific taxa on *S. aureus* have used
576 isolated pairs of strains, and here we expanded this to a broader community context.
577 Our work highlights how strain-level diversity, species co-occurrence, and metabolic
578 interactions collectively shape colonization outcomes.
579
580 *Limitations and Future Directions*
581 Our study has several limitations. First, our SynComs were assembled from a limited
582 culture collection of 10 species, which, while representing the most prevalent members
583 of the nasal microbiome, does not capture its full diversity. Fastidious or currently
584 unculturable taxa, not present in the LaCa collection, were necessarily excluded. Our
585 experimental setting did not reproduce the anaerobic microenvironments present in
586 the nasal cavity, and as a result two of the three anaerobic species failed to grow in
587 any SynCom. These anaerobes have been implicated in community structure and may
588 influence *S. aureus* dynamics [59]. Furthermore, only strains of *S. aureus* was used in
589 our invasion test. Use of other strains of *S. aureus* could help elucidate the strain-
590 dependent mechanisms of invasion success for this species.
591
592 Second, our experiments were performed entirely in vitro, which does not fully
593 recapitulate the nasal mucosal environment, host immune responses, or spatial
594 structure that may modulate microbial interactions and metabolite diffusion, as has
595 been shown for other microbial ecosystems. Future studies should expand SynCom

designs to include additional, fastidious species and incorporate host-derived factors such as epithelial cells, immune components, or human organoids, as has been done in porcine nasal microbiome models [24]. Incorporating physical structure into experimental setups is necessary, as it could help establish microaerophilic or anaerobic niches that support the growth of strict anaerobes and more closely mimic in vivo spatial organization which influences ecological interactions and dynamics [60, 61].

Finally, while our metabolomics analysis identified metabolites associated with specific community clusters, a substantial proportion of detected features remain unannotated, which limits mechanistic interpretation. Future work combining targeted metabolomics and genetic perturbations will be essential to confirm the specific roles of siderophores and amino acid competition in mediating *S. aureus* exclusion.

In summary, we demonstrate that nasal SynComs reproduce key compositional and functional features of the human nasal microbiome, including the emergence of distinct community states with variable resistance to *S. aureus* colonization. Our findings highlight the importance of both species and strain identity in shaping community assembly and function and suggest that nutritional competition particularly for iron and amino acids is a critical mechanism driving colonization resistance in a community context. These results provide a foundation for the rational design of microbiome-based interventions aimed at reducing *S. aureus* carriage and preventing infection. By integrating SynCom approaches with host-microbe models and in vivo validation, future research can further elucidate the ecological principles governing nasal microbiome stability and pathogen exclusion.

622 **Data availability**

623 Data is and R code for analyses are available on GitHub at: https://github.com/marcelo-
624 nd/nasalSynComs.

625

626 **References**

627 1. Caballero-Flores G, Pickard JM, Núñez G. Microbiota-mediated colonization
628 resistance: mechanisms and regulation. *Nat Rev Microbiol* 2023;**21**:347–360.
629 https://doi.org/10.1038/s41579-022-00833-7
630 2. Sarkar S et al. A Review on the Nasal Microbiome and Various Disease
631 Conditions for Newer Approaches to Treatments. *Indian J Otolaryngol Head*
632 *Neck Surg* 2023;**75**:755–763. https://doi.org/10.1007/s12070-022-03205-y
633 3. Sakr A et al. Staphylococcus aureus Nasal Colonization: An Update on
634 Mechanisms, Epidemiology, Risk Factors, and Subsequent Infections. *Front*
635 *Microbiol* 2018;**9**:2419. https://doi.org/10.3389/fmicb.2018.02419
636 4. Eiff CV, Peters G. Nasal Carriage as a Source of Staphylococcus aureus
637 Bacteremia. 2001.
638 5. Duhaniuc A et al. Multidrug-Resistant Bacteria in Immunocompromised Patients.
639 *Pharmaceuticals* 2024;**17**:1151. https://doi.org/10.3390/ph17091151
640 6. Chand U, Priyambada P, Kushawaha PK. Staphylococcus aureus vaccine
641 strategy: Promise and challenges. *Microbiological Research* 2023;**271**:127362.
642 https://doi.org/10.1016/j.micres.2023.127362
643 7. Van Dalen R et al. Secretory IgA impacts the microbiota density in the human
644 nose. *Microbiome* 2023;**11**:233. https://doi.org/10.1186/s40168-023-01675-y
645 8. Laux C, Peschel A, Krismer B. *Staphylococcus aureus* Colonization of the
646 Human Nose and Interaction with Other Microbiome Members. *Microbiol Spectr*
647 2019;**7**:7.2.34. https://doi.org/10.1128/microbiolspec.GPP3-0029-2018

648 9. Brugger SD et al. Dolosigranulum pigrum Cooperation and Competition in
649 Human Nasal Microbiota. *mSphere* 2020;**5**:e00852-20.
650 https://doi.org/10.1128/mSphere.00852-20
651 10. Krismer B et al. Nutrient Limitation Governs Staphylococcus aureus Metabolism
652 and Niche Adaptation in the Human Nose. *PLoS Pathog* 2014;**10**:e1003862.
653 https://doi.org/10.1371/journal.ppat.1003862
654 11. Tamkin E et al. Airway *Corynebacterium* interfere with *Streptococcus*
655 *pneumoniae* and *Staphylococcus aureus* infection and express secreted factors
656 selectively targeting each pathogen. *Infect Immun* 2025;**93**:e00445-24.
657 https://doi.org/10.1128/iai.00445-24
658 12. Krismer B et al. The commensal lifestyle of Staphylococcus aureus and its
659 interactions with the nasal microbiota. *Nat Rev Microbiol* 2017;**15**:675–687.
660 https://doi.org/10.1038/nrmicro.2017.104
661 13. Zhao Y et al. Nasal commensals reduce *Staphylococcus aureus* proliferation by
662 restricting siderophore availability. *The ISME Journal* 2024;**18**:wrae123.
663 https://doi.org/10.1093/ismejo/wrae123
664 14. Proctor DM, Relman DA. The Landscape Ecology and Microbiota of the Human
665 Nose, Mouth, and Throat. *Cell Host & Microbe* 2017;**21**:421–432.
666 https://doi.org/10.1016/j.chom.2017.03.011
667 15. Hardy BL, Merrell DS. Friend or Foe: Interbacterial Competition in the Nasal
668 Cavity. *J Bacteriol* 2021;**203**. https://doi.org/10.1128/JB.00480-20
669 16. Faith JJ et al. The Long-Term Stability of the Human Gut Microbiota. *Science*
670 2013;**341**:1237439. https://doi.org/10.1126/science.1237439
671 17. Venturelli OS et al. Deciphering microbial interactions in synthetic human gut
672 microbiome communities. *Molecular Systems Biology* 2018;**14**:e8157.
673 https://doi.org/10.15252/msb.20178157

674 18. Bai Y et al. Functional overlap of the Arabidopsis leaf and root microbiota.
675 *Nature* 2015;**528**:364–369. https://doi.org/10.1038/nature16192
676 19. Niu B et al. Simplified and representative bacterial community of maize roots.
677 *Proc Natl Acad Sci USA* 2017;**114**. https://doi.org/10.1073/pnas.1616148114
678 20. Goodman AL et al. Extensive personal human gut microbiota culture collections
679 characterized and manipulated in gnotobiotic mice. *Proc Natl Acad Sci USA*
680 2011;**108**:6252–6257. https://doi.org/10.1073/pnas.1102938108
681 21. Pacheco AR, Osborne ML, Segrè D. Non-additive microbial community
682 responses to environmental complexity. *Nat Commun* 2021;**12**:2365.
683 https://doi.org/10.1038/s41467-021-22426-3
684 22. Weiss AS et al. In vitro interaction network of a synthetic gut bacterial
685 community. *The ISME Journal* 2022;**16**:1095–1109.
686 https://doi.org/10.1038/s41396-021-01153-z
687 23. Buffie CG et al. Precision microbiome reconstitution restores bile acid mediated
688 resistance to Clostridium difficile. *Nature* 2015;**517**:205–208.
689 https://doi.org/10.1038/nature13828
690 24. Bonillo-Lopez L et al. Porcine nasal organoids to model interactions between the
691 swine nasal microbiota and the host. *Microbiome* 2025;**13**:131.
692 https://doi.org/10.1186/s40168-025-02088-9
693 25. Camus L et al. Tyrosine availability shapes Staphylococcus aureus
694 nasal colonization and interactions with commensal communities. *bioRxiv*
695 2025;2025.05.06.651429. https://doi.org/10.1101/2025.05.06.651429
696 26. Turnbaugh PJ et al. The Human Microbiome Project. *Nature* 2007;**449**:804–810.
697 https://doi.org/10.1038/nature06244

698 27. Estaki M et al. QIIME 2 Enables Comprehensive End-to-End Analysis of Diverse
699 Microbiome Data and Comparative Studies with Publicly Available Data. *CP in*
700 *Bioinformatics* 2020;**70**:e100. https://doi.org/10.1002/cpbi.100
701 28. Callahan BJ et al. DADA2: High-resolution sample inference from Illumina
702 amplicon data. *Nat Methods* 2016;**13**:581–583.
703 https://doi.org/10.1038/nmeth.3869
704 29. Camacho C et al. BLAST+: architecture and applications. *BMC Bioinformatics*
705 2009;**10**:421. https://doi.org/10.1186/1471-2105-10-421
706 30. Goldfarb T et al. NCBI RefSeq: reference sequence standards through 25 years
707 of curation and annotation. *Nucleic Acids Research* 2025;**53**:D243–D257.
708 https://doi.org/10.1093/nar/gkae1038
709 31. Seol D et al. Microbial Identification Using rRNA Operon Region: Database and
710 Tool for Metataxonomics with Long-Read Sequence. *Microbiol Spectr*
711 2022;**10**:e02017-21. https://doi.org/10.1128/spectrum.02017-21
712 32. Curry KD et al. Emu: species-level microbial community profiling of full-length
713 16S rRNA Oxford Nanopore sequencing data. *Nat Methods* 2022;**19**:845–853.
714 https://doi.org/10.1038/s41592-022-01520-4
715 33. Rice P, Longden I, Bleasby A. EMBOSS: The European Molecular Biology Open
716 Software Suite. *Trends in Genetics* 2000;**16**:276–277.
717 https://doi.org/10.1016/S0168-9525(00)02024-2
718 34. Schmid R et al. Integrative analysis of multimodal mass spectrometry data in
719 MZmine 3. *Nat Biotechnol* 2023;**41**:447–449. https://doi.org/10.1038/s41587-
720 023-01690-2
721 35. Nothias L-F et al. Feature-based molecular networking in the GNPS analysis
722 environment. *Nat Methods* 2020;**17**:905–908. https://doi.org/10.1038/s41592-
723 020-0933-6

724 36. Dührkop K et al. Systematic classification of unknown metabolites using high-
725 resolution fragmentation mass spectra. *Nat Biotechnol* 2021;**39**:462–471.
726 https://doi.org/10.1038/s41587-020-0740-8
727 37. Dührkop K et al. SIRIUS 4: a rapid tool for turning tandem mass spectra into
728 metabolite structure information. *Nat Methods* 2019;**16**:299–302.
729 https://doi.org/10.1038/s41592-019-0344-8
730 38. Maechler M et al. cluster: Cluster analysis basics and extensions (R package
731 version 2.1.1). 2021. 2021.
732 39. Rousseeuw PJ. Silhouettes: A graphical aid to the interpretation and validation of
733 cluster analysis. *Journal of Computational and Applied Mathematics*
734 1987;**20**:53–65. https://doi.org/10.1016/0377-0427(87)90125-7
735 40. Ritchie ME et al. limma powers differential expression analyses for RNA-
736 sequencing and microarray studies. *Nucleic Acids Research* 2015;**43**:e47–e47.
737 https://doi.org/10.1093/nar/gkv007
738 41. Wickham H. ggplot2 Elegant Graphics for Data Analysis, 2nd edn. Springer
739 Cham, 2016.
740 42. Gonze D et al. Multi-stability and the origin of microbial community types. *The*
741 *ISME Journal* 2017;**11**:2159–2166. https://doi.org/10.1038/ismej.2017.60
742 43. Estrela S et al. Functional attractors in microbial community assembly. *Cell*
743 *Systems* 2022;**13**:29-42.e7. https://doi.org/10.1016/j.cels.2021.09.011
744 44. Stubbendieck RM et al. Competition among Nasal Bacteria Suggests a Role for
745 Siderophore-Mediated Interactions in Shaping the Human Nasal Microbiota.
746 *Appl Environ Microbiol* 2019;**85**:e02406-18. https://doi.org/10.1128/AEM.02406-
747 18

748 45. Tran TH et al. Metabolic capabilities are highly conserved among human nasal-
749 associated *Corynebacterium* species in pangenomic analyses. *mSystems*
750 2024;**9**:e01132-24. https://doi.org/10.1128/msystems.01132-24
751 46. Lubrano P et al. Metabolic mutations reduce antibiotic susceptibility of E. coli by
752 pathway-specific bottlenecks. *Mol Syst Biol* 2025;**21**:274–293.
753 https://doi.org/10.1038/s44320-024-00084-z
754 47. Heilbronner S. Staphylococcus lugdunensis. *Trends in Microbiology*
755 2021;**29**:1143–1145. https://doi.org/10.1016/j.tim.2021.07.008
756 48. Cole AL et al. Nasal microbiome inhabitants with anti- *Staphylococcus aureus*
757 activity. *Microbiol Spectr* 2025;e01024-25.
758 https://doi.org/10.1128/spectrum.01024-25
759 49. Cisneros M et al. Synergistic inhibition of pneumococcal growth by
760 *Dolosigranulum pigrum* and *Corynebacterium pseudodiphtheriticum:* insights
761 into nasopharyngeal microbial interactions. *Microbiol Spectr* 2025;**13**:e00138-25.
762 https://doi.org/10.1128/spectrum.00138-25
763 50. Liu C-C et al. Defects in energy metabolism increase the susceptibility of
764 *Staphylococcus aureus* and its small colony variants (SCVs) to *Staphylococcus*
765 *lugdunensis* and lugdunin. *Microbiol Spectr* 2025;e01006-25.
766 https://doi.org/10.1128/spectrum.01006-25
767 51. Bessesen MT. Interventions targeting the nasal microbiome to eradicate
768 methicilin-resistant Staphylococcus aureus. *Clinical Microbiology and Infection*
769 2025;**31**:190–193. https://doi.org/10.1016/j.cmi.2024.10.022
770 52. Liu Q et al. Staphylococcus epidermidis Contributes to Healthy Maturation of the
771 Nasal Microbiome by Stimulating Antimicrobial Peptide Production. *Cell Host &*
772 *Microbe* 2020;**27**:68-78.e5. https://doi.org/10.1016/j.chom.2019.11.003

53. Adolf LA, Heilbronner S. Nutritional Interactions between Bacterial Species Colonising the Human Nasal Cavity: Current Knowledge and Future Prospects. *Metabolites* 2022;**12**:489. https://doi.org/10.3390/metabo12060489
54. Rosenstein R et al. The Staphylococcus aureus-antagonizing human nasal commensal Staphylococcus lugdunensis depends on siderophore piracy. *Microbiome* 2024;**12**:213. https://doi.org/10.1186/s40168-024-01913-x
55. Bongers T. The Maturity Index, the evolution of nematode life history traits, adaptive radiation and cp-scaling. *Plant and Soil* 1999;**212**:13–22.
56. Wang Y et al. Recovery of bacterial network complexity and stability after simulated extreme rainfall is mediated by K−/r-strategy dominance. *Applied Soil Ecology* 2024;**203**:105657. https://doi.org/10.1016/j.apsoil.2024.105657
57. Zheng W et al. The response patterns of r- and K-strategist bacteria to long-term organic and inorganic fertilization regimes within the microbial food web are closely linked to rice production. *Science of The Total Environment* 2024;**942**:173681. https://doi.org/10.1016/j.scitotenv.2024.173681
58. Bushman SD, Skaar EP. The exploitation of nutrient metals by bacteria for survival and infection in the gut. *PLoS Pathog* 2025;**21**:e1013580. https://doi.org/10.1371/journal.ppat.1013580
59. Lucas SK et al. Anaerobic Microbiota Derived from the Upper Airways Impact Staphylococcus aureus Physiology. *Infect Immun* 2021;**89**:e00153-21. https://doi.org/10.1128/IAI.00153-21
60. Vallespir Lowery N, Ursell T. Structured environments fundamentally alter dynamics and stability of ecological communities. *Proc Natl Acad Sci USA* 2019;**116**:379–388. https://doi.org/10.1073/pnas.1811887116

61. Junkins EN et al. Environmental structure impacts microbial composition and secondary metabolism. *ISME Communications* 2022;**2**:15. https://doi.org/10.1038/s43705-022-00097-5